

# Mesoscale Terrestrial Laser Scanning of Fluvial Gravel Surfaces

Chi-Kuei Wang, *Member, IEEE*, Fu-Chun Wu, Guo-Hao Huang, and Ching-Yi Lee

**Abstract**—Terrestrial laser scanning (TLS) point cloud data were gathered in the field of exposed gravel surfaces for sampling sites with a spatial extent of  $6\text{ m} \times 6\text{ m}$ . We propose in this letter a novel two-stage mean-based filter scheme for processing the point cloud to generate the digital surface model (DSM) at a resolution of 1 cm. To the authors' knowledge, this letter reports the first work of generating a DSM of a gravel surface of such a large spatial extent with high spatial resolution using TLS. The elevation variations attributed to gravel clasts and single grains can both be captured in the point cloud data. To eliminate data voids due to the obstruction of the line of sight, a multiple-scan strategy is employed, which includes four scans at the corners of the sampling site and two supplementary scans for the central  $2\text{ m} \times 2\text{ m}$  area. The resultant DSM exhibits good agreement with elevation profiles obtained using a traditional manual profiler. The proposed method is an effective tool for obtaining a quality DSM of fluvial gravel surfaces using TLS with fewer scans than previous study.

**Index Terms**—Digital surface model (DSM), gravel-bed river, point cloud, terrestrial laser scanning (TLS).

## I. INTRODUCTION

MEASUREMENTS of gravel-bed surfaces are crucial for the studies of fluvial processes concerning the variations of surface elevation and substrate texture. The hydraulic resistance exerted on the flow stems from the grain- and form-scale roughness of the gravel surface. An airborne laser scanner (ALS) can gather the elevation of a gravel surface for a large area [1]. The footprint of the ALS is  $\sim 15\text{ cm}$  on the ground; thus, the ALS is more suitable for the measurement of form-scale roughness rather than the grain-scale roughness. To verify the ALS data, the ground truth should cover a sufficiently large spatial extent. Gravel surface elevations have also been measured *in situ* using handheld medical laser scanners [2], [3] and close-range photogrammetry [4]–[6]. However, both these methods have only acquired gravel surface areas smaller than  $1.3\text{ m} \times 1.3\text{ m}$  [4]–[6]; the form-scale features of the gravel-bed

topography may have been overlooked [7], [8]. Therefore, there is a pressing need for an instrument that can be used to measure the gravel surface at a larger spatial extent with a sufficiently high resolution.

Terrestrial laser scanning (TLS), which is based on the laser ranging technique [9], has recently been employed for measurements of gravel surfaces [10], [11]. These studies revealed that TLS is a promising tool for obtaining detailed high-quality 2-D elevations of gravel surfaces.

In this letter, we present a two-stage mean-based filter scheme by considering the elevation variation of the point cloud within each  $1\text{ cm} \times 1\text{ cm}$  cell to generate the digital surface model (DSM) of the gravel surface with a spatial extent of  $6\text{ m} \times 6\text{ m}$  and a spatial resolution of 1 cm. The fidelity of the resultant DSM is confirmed with elevation profiles gathered using a manual profiler. The results reveal that the proposed method is an effective tool for gathering the DSM information that may be further used to estimate the grain- and form-scale roughness of gravel surfaces.

## II. MATERIAL AND METHODS

### A. Study Sites

The study sites are located at a gravel bar near the confluence of the Nan-Shih River and the Pei-Shih River, northern Taiwan (latitude and longitude of  $24^\circ 54' 11''$  and  $121^\circ 33' 22''$ , respectively). The laser scans of the gravel bar surface were implemented at three  $6\text{ m} \times 6\text{ m}$  sampling sites, referred to as sites 96I, 97I, and 97II, respectively. The scans of 96I were carried out on October 26, 2007, whereas the scans of 97I and 97II were performed on January 30, 2008. The grain size distributions and the characteristic sizes (e.g.,  $D_{90}$ , which means that 90% of the gravels are smaller than this size) were obtained using the photosieving technique [12] with image samples taken from a  $50\text{ cm} \times 50\text{ cm}$  frame. The results indicate that the surface grains of 97I and 97II are coarser than those of 96I, with  $D_{90}$  values of 84.5, 105.0, and 101.8 mm for 96I, 97I, and 97II, respectively. Moreover, the surface grains of 97II are better sorted than those of 96I and 97I, with the sorting indexes being 2.11, 2.10, and 1.82 mm for 96I, 97I, and 97II, respectively. Fig. 1 shows the field conditions for 97I.

### B. TLS

TLS collects the 3-D points, or the so called point cloud, of a surface by measuring the range between the surface and the scanner with a transmitted laser beam that is directed with a high angular accuracy [13], [14]. For each scan, the coordinate origin is within the TLS system. The integration

Manuscript received January 5, 2011; revised April 13, 2011; accepted May 11, 2011. This work was supported in part by the National Science Council of Taiwan under Grant NSC100-2119-M-006-010 and in part by the Landmark Project of National Cheng Kung University, Tainan, Taiwan.

C.-K. Wang and G.-H. Huang are with the Department of Geomatics, National Cheng Kung University, Tainan 70101, Taiwan (e-mail: chikuei@mail.ncku.edu.tw; p6894101@mail.ncku.edu.tw).

F.-C. Wu is with the Department of Bioenvironmental Systems Engineering, National Taiwan University, Taipei 10617, Taiwan (e-mail: fcwu@ntu.edu.tw).

C.-Y. Lee was with National Cheng Kung University, Tainan 70101, Taiwan. She is now with the Land Administration Bureau of Taichung City Government, Taichung 40343, Taiwan (e-mail: jing0304@yahoo.com.tw).

Color versions of one or more of the figures in this paper are available online at <http://ieeexplore.ieee.org>.

Digital Object Identifier 10.1109/LGRS.2011.2156758

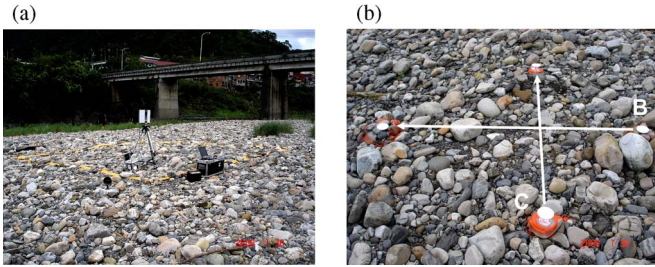


Fig. 1. (a) Field photograph of 97I (bounded by the yellow lines). Four circular scanner targets were placed around the  $6\text{ m} \times 6\text{ m}$  area. (b) Close-up photograph of the central  $2\text{ m} \times 2\text{ m}$  area of 97I. The arrows pointing left and up are profiles B and C, respectively. The two profiles are both  $2.2\text{ m}$  long.

of multiple scans is facilitated by the use of circular marks of high reflection contrast [Fig. 1(a)] and is processed with the commercial software Cyclone (Leica Geosystems).

Two TLS systems, HDS3000 and HDS4500 (Leica Geosystems), were used in this study. HDS3000 was used in the scans of 96I, and HDS4500 was employed in the scans of 97I and 97II. The position accuracy of these two systems is  $6\text{ mm}$  within the distance range of  $10\text{ m}$ , and the precision is better than  $2\text{ mm}$ , which makes them suitable for gathering gravel surface geometry [10].

### C. Multiple-Scan Strategy

A multiple-scan strategy was implemented in this study to eliminate data voids that are due to the obstructed line of sight by large protruding grains. The laser scanning was carried out at the four corners of the  $6\text{ m} \times 6\text{ m}$  sampling area. Two extra scans were performed at the two corners of the central  $2\text{ m} \times 2\text{ m}$  region along one diagonal of the  $6\text{ m} \times 6\text{ m}$  sampling area. The scanner was set up  $1\text{ m}$  away from the corners of the sampling area to maximize the area covered by a single scan. The outer scans were followed by the inner scans to avoid disturbing the gravels. The rotation speeds of the scanner were such that the point cloud density of the individual scans was at least  $\sim 1\text{ point/cm}^2$ , from which a DSM with  $1\text{-cm}$  resolution can be obtained if the entire gravel surface is visible with a single scan. The inner scans were, however, set to much slower speeds to obtain point cloud densities of  $\sim 10\text{ points/cm}^2$  for the individual scans.

To facilitate the registration of these six scans, four circular scanner targets with an alternating black and white pattern were placed approximately equidistant from each other around the perimeter that extends  $2\text{ m}$  away from the  $6\text{ m} \times 6\text{ m}$  sampling area [Fig. 1(a)]. The mean absolute errors of the registration results for all three sites are better than  $3\text{ mm}$ .

### D. DSM Generation

Integrating the results of multiple scans leads to a dense point cloud that represents the gravel surface. Fig. 2(a) shows the point cloud obtained within a region of  $25\text{ cm}$  (long)  $\times 1\text{ cm}$  (width). Unlike the elevation profile that would be extracted from a DSM, which is a series of elevations at fixed intervals along a line over the gravel surface, TLS randomly records the 3-D information of the gravel surface as a result of its scan patterns [15]. Fig. 2(b) shows a schematic 3-D plot demonstrating the difference between the elevation profile extracted from a

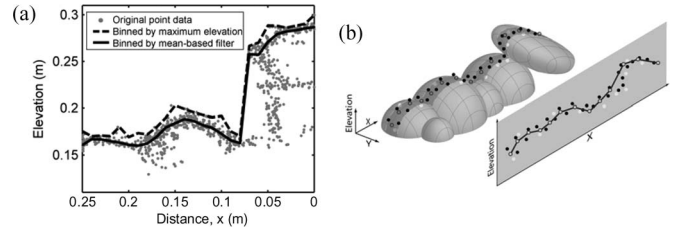


Fig. 2. (a) Comparison of DSMs binned by maximum elevation [2] and mean-based filter scheme. (b) Schematic 3-D plot demonstrating the difference between the elevation profile extracted from a DSM and a point cloud obtained from TLS. The grid lines overlaid on the gravel surface correspond to  $1\text{ cm} \times 1\text{ cm}$  cells. The open circles denote the elevation obtained from a DSM. The black and white circles denote TLS point clouds scattered above and below the gravel surface, respectively.

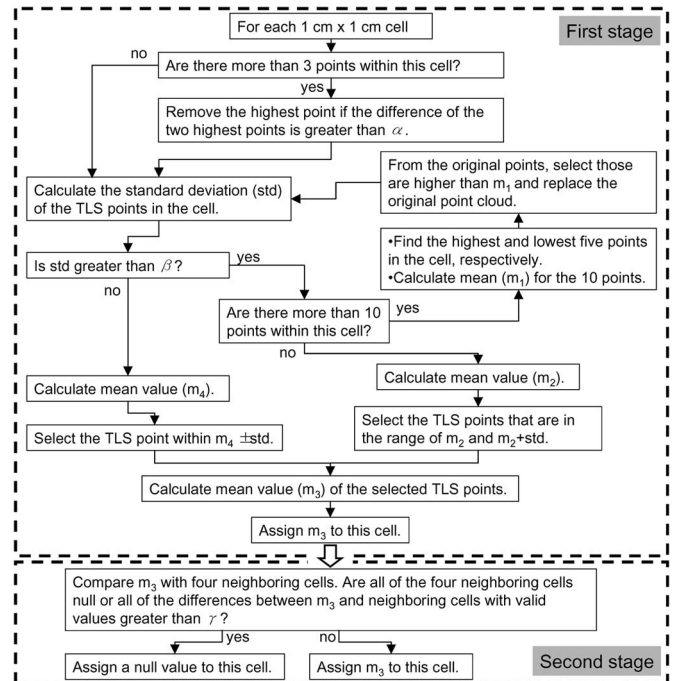


Fig. 3. Flowchart of the proposed two-stage mean-based filter.

DSM and the point cloud obtained from TLS. The grid lines overlaid on the gravel surface correspond to  $1\text{ cm} \times 1\text{ cm}$  cells. The open circles denote the surface profile extracted from a DSM, whereas the black and white circles denote point clouds that are above and below, respectively, the “true” gravel surface due to the measurement variability intrinsic to TLS [9], [13].

As the gravel surface is unlikely to be distinctly portrayed by the point cloud data, it is necessary to devise a filter and bin the point cloud into cells of an appropriate size [10]. In this study, a cell size of  $1\text{ cm} \times 1\text{ cm}$  was used. Binning the point cloud of the gravel surface using the maximum elevation within the cell as the representative [2] does not produce a satisfactory DSM because it produces a fluctuating and jerky surface profile and thus tends to roughen the bed surface [see the dashed line in Fig. 2(a)].

To address the aforementioned issues, we developed a two-stage mean-based filter scheme for point data obtained from TLS (Fig. 2). In the first stage, the flying errors, or mixing pixel errors [10], are eliminated by removing the highest point if the difference between the highest two points in a cell is greater

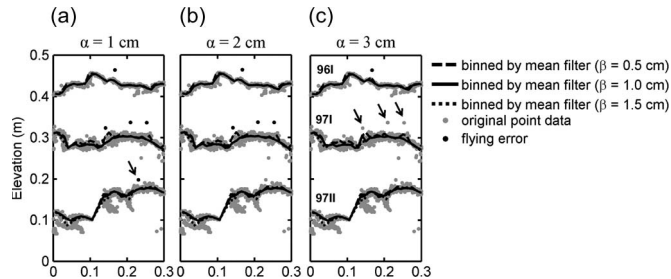


Fig. 4. Flying errors identified with (a)  $\alpha = 1$  cm, (b)  $\alpha = 2$  cm, and (c)  $\alpha = 3$  cm and TLS-derived DSMs with various  $std$  thresholds  $\beta$  for three example profiles extracted from 96I, 97I, and 97II. See the text for the explanation of the arrows.

than a threshold  $\alpha$ . Flying errors appear as isolated points elevated unusually high above the clustered point depicting the gravel surface. The black dots in Fig. 4 show the flying errors that are identified with various  $\alpha$  thresholds for three example profiles that are extracted from 96I, 97I, and 97II. When  $\alpha = 1$  cm, the point cloud that is slightly elevated above the surface is misidentified as a flying error [the arrow in Fig. 4(a)]; when  $\alpha = 3$  cm, the flying errors are missed [the arrows in Fig. 4(c)]. Thus, the threshold value of  $\alpha$  is 2 cm for the study sites in order to maximize and to minimize the identification of flying errors simultaneously. The point data in each cell are then iteratively examined, and those that may represent hidden surfaces of the gravels are filtered out. The standard deviation ( $std$ ) of the elevations of all points within a cell is used as the criterion for filtering. If the  $std$  is greater than a specified threshold  $\beta$ , implying that hidden-surface data may be present, the number of data points within the cell is further checked. If there are more than ten points within the cell, five of the greatest and smallest elevations are used to calculate a mean value  $m_1$ . Points with elevations greater than  $m_1$  are taken to be potentially on the top surface. The original point cloud is replaced by the potential top-surface points, and the procedure is repeated until the updated  $std$  is less than the specified threshold. When fewer than ten points are within the cell, a mean elevation  $m_2$  of the points is calculated, and the top-surface elevation  $m_3$  is estimated and assigned to the cell by averaging the point data that are within  $m_2$  and  $m_2 + std$ . If the  $std$  is less than  $\beta$ , the estimation of the top-surface elevation  $m_3$  is straightforward; it includes the calculation of the mean elevation  $m_4$  of the point data and the averaging of the point data that are within  $m_4 \pm std$ . Fig. 4 shows the TLS-derived DSMs for  $std$  thresholds of 0.5, 1, and 1.5 cm for three example profiles extracted from 96I, 97I, and 97II. When the  $std$  threshold is 0.5 cm, the TLS-derived DSM becomes jerky and has the tendency to track the noisy point data that are higher than the gravel surface (the dashed line in Fig. 4(b) for 97I at  $x = 0.15$  m). On the other hand, when the  $std$  threshold is 1.5 cm, the TLS-derived DSM fails to depict the edge of the gravel surface at  $x = 0.05$  m for 97I and at  $x = 0.05$  m for 97II [the dotted lines in Fig. 4(b)]. For this reason, the  $std$  threshold is 1 cm for the study sites.

In the second stage, the outliers of the measurements that were not filtered in the first stage are eliminated. This is achieved by comparing the  $m_3$  value of a cell with the  $m_3$  values of its four neighboring cells. If all of the four neighbors are null or the four differences with the  $m_3$  value are all greater

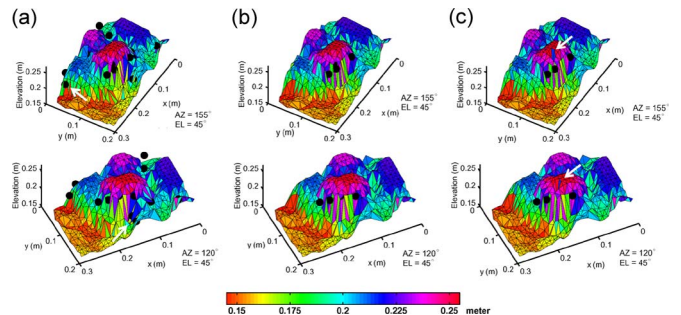


Fig. 5. Three-dimensional visualization of the TLS-derived DSM with two sets of horizontal rotation ( $AZ$ ) and vertical elevation ( $EL$ ) angles. The dots are outliers identified with (a)  $\gamma = 1$  cm, (b)  $\gamma = 2$  cm, and (c)  $\gamma = 3$  cm. See the text for the explanation of the arrows.

than the specified threshold  $\gamma$ , a null value is assigned to the cell because its  $m_3$  value was very likely subjected to flying error or system error. The dots in Fig. 5 show that the remaining outliers are isolated high points in a 3-D visualization environment for a small patch of  $0.3 \text{ m} \times 0.2 \text{ m}$  with various  $\gamma$  threshold values and with two viewing perspectives; the gravel surface shows smooth variation. When  $\gamma = 1$  cm, many of the point clouds are misidentified as outliers [the arrows in Fig. 5(a)] as they are very close to the gravel surface. When  $\gamma = 3$  cm, a deep hole appears at the center of a gravel [the arrows in Fig. 5(c)] caused by point data of lower elevation value due to the TLS system error. Thus, the threshold value of  $\gamma$  is 2 cm. The surface profiles obtained using the proposed filter scheme are shown in Figs. 2(a) and 4(b) as solid lines, which portray more plausible profiles of the gravel surface.

### E. Manual Surface Profile Collection

To assess the fidelity of the TLS-derived DSM, we used a manual profiler to measure three surface profiles along the longitudinal and transverse centerlines of the study sites. The manual profiler used a 15-cm point pin (with a diameter of 2 mm at the tip) that was extended from a leveling rod. Two levels with ticks were set up in parallel approximately 45 and 85 cm above the ground, respectively. The leveling rod was kept vertical during the manual measurements by pressing it against the two levels and stepping forward with the same number of ticks on the two levels. The elevations were recorded to the nearest millimeter, and profiles were measured at 1-cm intervals.

## III. RESULTS AND DISCUSSION

### A. TLS-Derived DSM

For each of the three  $6 \text{ m} \times 6 \text{ m}$  sampling sites, more than 2.75 million data points were collected (Table I) with a point cloud density consistently over  $7.64 \text{ points/cm}^2$ . Due to the obstruction of the line of sight by large pieces of gravel, the ground was not fully covered by the point data from the nadir perspective, despite using the proposed multiple-scan strategy. The TLS-derived DSMs of the three sites are shown as shaded relief maps in Fig. 6. Fewer data voids are observed in the central  $2 \text{ m} \times 2 \text{ m}$  regions where the supplemental scan data with a higher angle of incidence were used. The point density of the supplemental scans ranging

TABLE I  
TLS RESULTS FOR THE THREE STUDY SITES

Site	Number of data points		Point cloud density (points/cm <sup>2</sup> )		DSM coverage (%)	
	(6 m × 6 m)	(2 m × 2 m)	(6 m × 6 m)	(2 m × 2 m)	(6 m × 6 m)	(2 m × 2 m)
96I	3,068,293	385,402	8.80	9.63	93.9	98.2
97I	3,019,091	1,071,102	8.39	26.70	76.4	97.6
97II	2,750,439	883,063	7.64	22.08	82.6	98.5

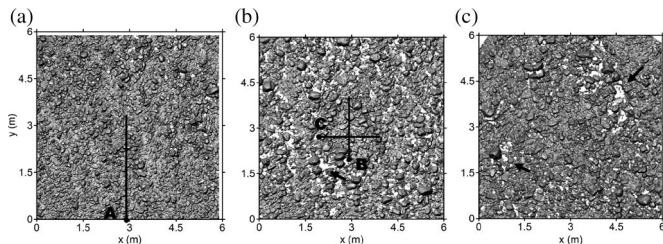


Fig. 6. Shaded relief maps of the TLS-derived DSMs for (a) 96I, (b) 97I, and (c) 97II. The solid lines are profiles A, B, and C; the solid circles at the ends are the origins of the profiles. The field photograph including profiles B and C is shown in Fig. 1(b). The arrows indicate data voids due to the obstruction of the line of sight by large pieces of gravel.

from 9.63 to 26.7 points/cm<sup>2</sup> was consistently greater than those of the first four scans. The DSM coverage, defined as the ratio of the number of cells with a valid DSM, which refers to that produced by the proposed filter scheme, to the total number of cells, ranged from 76.4% to 93.9% for the 6 m × 6 m areas but was consistently greater than 97.6% for the 2 m × 2 m areas.

The DSM coverage of the 6 m × 6 m area is affected by the size and sorting property of the gravels. For example, the DSM coverage of 96I (93.2%) is higher than that of 97I (76.4%) as the grain size of 96I ( $D_{90} = 84.5$  mm) is smaller than that of 97I ( $D_{90} = 105.0$  mm), while they have similar sorting indexes (the values are 2.11 and 2.10 mm for 96I and 97I, respectively). For the examples of 97I and 97II, the DSM coverage of 97II (82.6%) is higher than that of 97I (76.4%) as the sorting index of 97II (1.82 mm) is smaller than that of 97I (2.10 mm), while they have similar grain sizes (the  $D_{90}$  values are 105.0 and 101.8 mm for 97I and 97II, respectively). The lowest DSM coverage of 97I is due to the combination of large grain size ( $D_{90} = 105$  mm) and large sorting index (2.10 mm).

A comparison of the shaded relief maps reveals that 96I was covered by more homogeneous and small gravel, resulting in fewer obstructed inaccessible spots and, thus, a high DSM coverage. In contrast, larger gravel at 97I and 97II is associated with greater patches of data voids, as indicated by the arrows in Fig. 6. With the two supplemental scans, however, the voids in the central 2 m × 2 m region were significantly reduced.

### B. Assessment of the TLS-Derived DSM

Three manual elevation profiles of the gravel surface are denoted as A, B, and C in Fig. 6, respectively; the solid circles at the ends are the origins of the profiles. The resulting surface profiles are shown in Fig. 7(a) as gray lines. The corresponding elevation profiles were extracted from the TLS-derived DSMs. They are shown in Fig. 7(a) as black lines.

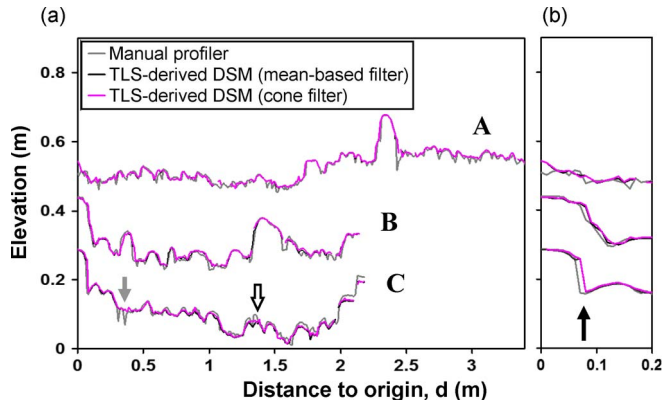


Fig. 7. (a) Comparison of surface elevation profiles obtained by a manual profiler and extracted from the TLS-derived DSM. The cone filter is adopted from [10]. (b) Magnified view of (a). The gray arrow shows the difference of elevation due to the limited accessibility by TLS. The black arrow shows the difference of elevation at the side face of the gravel. The hollow arrow shows the difference between the cone-filter-derived DSM and the mean-based-derived DSM and the manual profile.

TABLE II  
COMPARISON OF REGRESSION RESULTS IN  
FIG. 7 FOR PROFILES A, B, AND C

	Mean-based filter			Cone filter <sup>a</sup>		
	A	B	C	A	B	C
Slope	0.9687	1.015	0.9542	0.9628	1.018	0.9583
Intercept	0.0137	-0.0068	0.0087	0.016	-0.01	0.006
R <sup>2</sup>	0.966	0.955	0.951	0.952	0.954	0.956
Reduced major axis regression						
Slope	0.9943	0.9928	1.021	0.9928	0.986	1.005
R <sup>2</sup>	0.965	0.955	0.945	0.951	0.953	0.953

<sup>a</sup> adopted from [10]

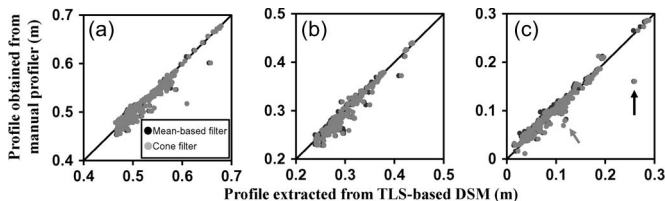


Fig. 8. Scatter plots showing a comparison of surface elevation profiles A, B, and C obtained by a manual profiler and extracted from the TLS-derived DSM. The gray and black arrows are the same as those in Fig. 7.

Overall, the TLS-derived surface profiles shown in Fig. 7(a) agree well with the corresponding profiles obtained by using a manual profiler. Table II shows the coefficients of determination  $R^2$  of the reduced major axis regression for profiles A, B, and C being 0.965, 0.955, and 0.945, respectively, as they are centered around the one-to-one line in the scatter plots shown in Fig. 8. There are, however, a few noticeable data points that do not match and are worth mentioning here. The first is exemplified by the two points in profile C at  $d \approx 0.3$  m [indicated by the gray arrows in Figs. 7(a) and 8(c)], where the elevations obtained by the manual profiler are apparently ( $\sim 4$  cm) lower than those extracted from the TLS-derived DSM. This discrepancy is attributed to small areas that were reachable by the manual profiler but inaccessible to the laser scanner, even with the implementation of multiple scans.

The second is the difference observed in profile C at  $d = \sim 0.1$  m [indicated by the black arrows in Figs. 7(b) and 8(c)], where the elevation extracted from the TLS-derived DSM is much greater than that obtained by the manual profiler. Such difference was observed at the side face of the gravel. The proposed filter scheme tracked the mean elevation of the top surface at the center of a cell, where the manual profiler measured the elevation with a pin point. The edge boundary determined by the two methods can differ by up to 1 cm. This was, however, a rare situation, and only a few cases were observed in the profiles presented here.

At last, discrepancies may be caused by the misalignment of the leveling rod. The two levels used to ensure the vertical configuration of the leveling rod were made of aluminum; they slightly deformed when subjected to external forces during the measurements. Such discrepancies were repeatedly observed in profile C from  $d = 2$  to 2.2 m [Fig. 7(a)].

A similar filter for producing DSM for gravel surfaces using TLS was developed in [10]. The filter consists of three steps, namely, the repeat-scan error value (RSEV) filter followed by a cone filter and a local high point filter. The RSEV filter effectively removes mixing errors with a prerequisite of a minimum of three repeated scans at each scan location. Because our data were collected prior to the publication of [10], repeated scans were not available for the RSEV filter. Thus, for the comparison, the prominent mixing errors were removed using the proposed  $\alpha$  threshold (Fig. 3). Since the local high point filter [10] is very similar to the  $\gamma$  threshold, the major difference between the proposed filter and that in [10] should result from the cone filter. We implemented the cone filter and used it after the  $\alpha$  threshold in the first stage (Fig. 3). The corresponding elevation profiles A, B, and C from the cone-filter-derived DSMs are shown in Fig. 7(a) as magenta lines. The coefficients of determination  $R^2$  of the reduced major axis regression are 0.951, 0.953, and 0.953 for profiles A, B, and C, respectively, as they are centered around the one-to-one line in the scatter plots shown in Fig. 8. The  $R^2$  values for the mean-based filter are better than those for the cone filter, except for profile C. The scatter plot in Fig. 8 shows very similar distributions of DSM results for the two filters. One noticeable difference is indicated by the hollow arrow in Fig. 7(a) at  $d = 1.4$  m, where the manual profiler and the mean-based TLS-derived DSM both depicts a trough of the gravel surface, but the cone-filter-based TLS-derived DSM failed to do so. Thus, the proposed filter outperforms the cone filter and requires fewer scans.

#### IV. CONCLUSION

A two-stage mean-based filter scheme for processing TLS point clouds has been proposed for generating a DSM of fluvial gravel surfaces. Most of the data voids were located around larger pieces of gravel, where the accessibility of TLS is obstructed by the protruding gravels. Fewer data voids were

observed in the central regions where the supplemental scan data were used. Overall, the TLS-derived surface profiles are in satisfactory agreement with the corresponding profiles obtained using a manual profiler. The proposed method is an effective tool for obtaining a quality DSM that may be employed to further quantify the grain- and form-scale roughness of gravel surfaces.

#### ACKNOWLEDGMENT

The authors would like to thank Control Signal Company, Ltd., New Taipei City, 23145 Taiwan, for their field work assistance. The reviews from the five anonymous referees and the associate editor have improved this letter significantly.

#### REFERENCES

- [1] Y.-L. Lin and C.-K. Wang, "Assessment of airborne lidar data for instream flow type classification," in *Proc. IEEE Int. Geosci. Remote Sens. Symp.*, Honolulu, HI, 2010, pp. 930–933.
- [2] V. Nikora and J. Walsh, "Water-worked gravel surfaces: High-order structure functions at the particle scale," *Water Resour. Res.*, vol. 40, p. W12601, Dec. 2004.
- [3] G. Smart, J. Aberle, M. Duncan, and J. Walsh, "Measurement and analysis of alluvial bed roughness," *J. Hydraul. Res.*, vol. 42, pp. 227–237, Mar. 2004.
- [4] J. B. Butler, S. N. Lane, and J. H. Chandler, "Assessment of DEM quality for characterizing surface roughness using close range digital photogrammetry," *Photogramm. Rec.*, vol. 16, no. 92, pp. 271–291, Oct. 1998.
- [5] J. B. Butler, S. N. Lane, and J. H. Chandler, "Characterization of the structure of river-bed gravels using two-dimensional fractal analysis," *Math. Geol.*, vol. 33, no. 3, pp. 301–330, Apr. 2001.
- [6] P. E. Carbonneau, S. N. Lane, and N. E. Bergeron, "Cost-effective non-metric close-range digital photogrammetry and its application to a study of coarse gravel river beds," *Int. J. Remote Sens.*, vol. 24, no. 14, pp. 2837–2854, Jul. 2003.
- [7] C. De Jong, "Measuring changes in micro and macro roughness on mobile gravel beds," in *Proc. Erosion Sediment Transp. Monit. Programmes River Basins*, Oslo, Norway, 1992, pp. 31–40.
- [8] V. I. Nikora, D. G. Goring, and B. J. F. Biggs, "On gravel-bed roughness characterization," *Water Resour. Res.*, vol. 34, no. 3, pp. 517–527, Oct. 1998.
- [9] E. P. Baltsavias, "Airborne laser scanning: Basic relations and formulas," *ISPRS J. Photogramm. Remote Sens.*, vol. 54, no. 2/3, pp. 199–214, Jul. 1999.
- [10] R. Hodge, J. Brasington, and K. Richards, "In situ characterization of grain-scale fluvial morphology using terrestrial laser scanning," *Earth Surf. Process. Land.*, vol. 34, no. 7, pp. 954–968, Jun. 2009.
- [11] G. L. Heritage and D. J. Milan, "Terrestrial laser scanning of grain roughness in a gravel-bed river," *Geomorphology*, vol. 113, no. 1/2, pp. 4–11, Dec. 2009.
- [12] D. J. Graham, S. P. Rice, and I. Reid, "A transferable method for the automated grain sizing of river gravels," *Water Resour. Res.*, vol. 41, p. 12, Jul. 2005.
- [13] D. D. Lichti, S. J. Gordon, and T. Tipdecho, "Error models and propagation in directly georeferenced terrestrial laser scanner networks," *J. Surv. Eng.-ASCE*, vol. 131, no. 4, pp. 135–142, Nov. 2005.
- [14] F. M. Danson, D. Hetherington, F. Morsdorf, B. Koetz, and B. Allgower, "Forest canopy gap fraction from terrestrial laser scanning," *IEEE Geosci. Remote Sens. Lett.*, vol. 4, no. 1, pp. 157–160, Jan. 2007.
- [15] Y. W. Choi, Y. W. Jang, H. J. Lee, and G. S. Cho, "Three-dimensional LiDAR data classifying to extract road point in urban area," *IEEE Geosci. Remote Sens. Lett.*, vol. 5, no. 4, pp. 725–729, Oct. 2008.